

Targeting IKK ϵ in Androgen-Independent Prostate Cancer Causes Phenotypic Senescence and Genomic Instability



Sophie Gilbert¹, Benjamin Péant¹, Nicolas Malaquin¹, Véronique Tu¹, Hubert Fleury¹, Kim Leclerc-Desaulniers¹, Francis Rodier^{1,2}, Anne-Marie Mes-Masson^{1,3}, and Fred Saad^{1,4}

ABSTRACT

Advanced prostate cancer will often progress to a lethal, castration-resistant state. We previously demonstrated that IKK ϵ expression correlated with the aggressiveness of prostate cancer disease. Here, we address the potential of IKK ϵ as a therapeutic target in prostate cancer. We examined cell fate decisions (proliferation, cell death, and senescence) in IKK ϵ -depleted PC-3 cells, which exhibited delayed cell proliferation and a senescent phenotype, but did not undergo cell death. Using IKK ϵ /TBK1 inhibitors, BX795 and Amlexanox, we measured their effects on cell fate decisions in androgen-sensitive prostate cancer and androgen-independent prostate cancer cell lines. Cell-cycle analyses revealed a G₂-M cell-cycle arrest and a higher proportion of cells with 8N DNA

content in androgen-independent prostate cancer cells only. Androgen-independent prostate cancer cells also displayed increased senescence-associated (SA)- β -galactosidase activity; increased γ H2AX foci; genomic instability; and altered p15, p16, and p21 expression. In our mouse model, IKK ϵ inhibitors also decreased tumor growth of androgen-independent prostate cancer xenografts but not 22Rv1 androgen-sensitive prostate cancer xenografts. Our study suggests that targeting IKK ϵ with BX795 or Amlexanox in androgen-independent prostate cancer cells induces a senescence phenotype and demonstrates *in vivo* antitumor activity. These results strengthen the potential of exploiting IKK ϵ as a therapeutic target.

Introduction

Prostate cancer is the most frequently diagnosed cancer in North American men. Androgen deprivation therapy (ADT) is the standard of care for advanced prostate cancer. However, most patients with hormone-sensitive prostate cancer (HSPC) eventually progress to the more aggressive and lethal form of the disease, castration-resistant prostate cancer (CRPC). Mutations and aberrant expression of the androgen receptor (AR; refs. 1–4) as well as non-AR-related pathways are associated with the development of CRPC. However, the molecular events that lead to this progression are still largely unknown and likely multifactorial. A better understanding of these mechanisms is needed to identify new therapeutic targets and treatment strategies for prostate cancer that is no longer responsive to ADT in order to improve patient outcomes.

IKK ϵ is a member of the IKK family and associates with the TANK-binding kinase (TBK1) to induce an immune response that involves Toll-like receptor 3 (TLR3)- and TLR4-mediated IFN production through the phosphorylation of IFN regulatory factors (IRFs), IRF3 and IRF7 (5). IKK ϵ overexpression in prostate, breast, ovarian, and lung cancers can result in the deregulation of its different targets (6–8). Péant and colleagues showed that IKK ϵ overexpression results in phosphorylation and nuclear translocation of the transcription factor CAAT/enhancer binding protein (C/EBP)- β , leading to transcription of IL6 and contributing to inflammation, cell proliferation, progression to CRPC, and the development of bone metastases (9, 10). In addition, CRPC as modelled by androgen-independent prostate cancer cell lines is associated with the constitutive expression of IKK ϵ that is dependent on NF- κ B signaling (11). It was shown that AR activation induces the expression of I- κ B α , which in turn, inhibits the NF- κ B canonical pathway resulting in the failure to constitutively express IKK ϵ in androgen-sensitive prostate cancer cell lines (11). Péant and colleagues also showed that depletion of IKK ϵ expression decreased androgen-independent prostate cancer cell proliferation and tumor volume in a mouse model (12). Furthermore, IKK ϵ expression directly correlates with aggressive prostate cancer disease in patients (9). These findings show that IKK ϵ has an oncogenic role in prostate cancer and suggest its potential as a therapeutic target for CRPC.

Recent studies have shown that C/EBP- β participates in the development of senescence in prostate cancer cells in response to ADT, known as androgen deprivation-induced senescence (ADIS). Cellular senescence is a state of stable cell-cycle arrest induced by stress. In cancer, senescence plays a dual role that is either antitumorigenic by stimulating the immune system (13, 14) or protumorigenic by inducing apoptosis resistance or the senescence-associated secretory phenotype (SASP; ref. 15). Burton and colleagues demonstrated that prostate cancer cells in ADIS were enhanced in protumoral activities that involved prosurvival mechanisms and chemoresistance (10). In addition, Pernicova and colleagues showed a relationship between the inhibition of AR signaling and formation of tumor-promoting

¹Centre de recherche du Centre hospitalier de l'Université de Montréal (CRCHUM) et Institut du cancer de Montréal, Montréal, Quebec, Canada.

²Département de Radiologie, Radio-oncologie et Médecine Nucléaire, Université de Montréal, Montreal, Quebec, Canada. ³Faculty of Medicine, Université de Montréal, Montreal, Quebec, Canada. ⁴Department of Surgery, Université de Montréal, Montreal, Quebec, Canada.

Note: Supplementary data for this article are available at Molecular Cancer Therapeutics Online (<http://mct.aacrjournals.org/>).

Corresponding Author: Anne-Marie Mes-Masson, Centre de recherche du Centre Hospitalier de l'Université de Montréal (CRCHUM) et Institut du cancer de Montréal, 900 Saint Denis Street, Montreal, Quebec H2X 0A9, Canada. Phone: 514-890-8000, ext. 25496; E-mail: anne-marie.mes-masson@umontreal.ca

Mol Cancer Ther 2022;21:407-18

doi: 10.1158/1535-7163.MCT-21-0519

This open access article is distributed under Creative Commons Attribution-NonCommercial-NoDerivatives License 4.0 International (CC BY-NC-ND).

©2021 The Authors; Published by the American Association for Cancer Research

senescent cells through the downregulation of the S-phase kinase-associated protein 2 (Skp2; ref. 16).

To elucidate the role of IKK ϵ in the progression of prostate cancer, we treated prostate cancer cell lines with the IKK ϵ /TBK1 inhibitors, BX795, and Amlexanox, and examined the resulting cell fate decisions, such as senescence and cell death. BX795 and Amlexanox blocked IKK ϵ activity in prostate cancer cell lines, independent of TBK1 and reduced cell proliferation with features of senescence mediated by IKK ϵ in androgen-independent prostate cancer cells. At a high concentration, BX795 induced greater genomic instability and mitotic catastrophe that led to senescence and cell death. Using preclinical xenograft models, we showed that BX795 or Amlexanox treatment slowed the progression of tumor growth in androgen-independent prostate cancer xenografts, demonstrating a potential in targeting IKK ϵ for novel androgen-independent prostate cancer interventions and treatment.

Materials and Methods

Cell lines and cell culture

PC cell lines PC-3, DU145, LNCaP, and 22Rv1 and the normal prostate cell line PZ-HPV-7 were purchased from the ATCC (CRL1435, ATCC HTB-81, ATCC CRL-174, and ATCC CRL-250, respectively). The prostate cancer cell line C4-2B was kindly provided by Dr. Martin Gleave (Vancouver Prostate Center). Cells were cultured in RPMI 1640 (Wisent Inc.) supplemented with 10% FBS, 100- μ g/mL gentamicin, and 0.25- μ g/mL amphotericin B (Invitrogen). Prior to beginning the study, cell lines were validated by short tandem repeat DNA profiling.

Drugs

BX795 was purchased from Invitrogen, and Amlexanox was purchased from Abcam. Drugs were dissolved in 100% DMSO and then further diluted in complete RPMI media for *in vitro* experiments. Drugs were added 24 hours after seeding.

Cloning, viruses, and infections

The lentiviral short hairpin RNA (shRNA) against IKK ϵ (shIKK ϵ .A: 5'-ATGGCTATCGTGTGGGCA-3'; shIKK ϵ .B: 5'-CGAAA-CATTAGCTCCTGCCA-3') and red fluorescent protein (RFP; control; shRFP: 5'-ACTACACCATCGTGGACAGT-3') were purchased from Dharmacon (lentiviral PLKO.1 vector with puromycin selection). Viruses were produced as previously described (17), and titers were adjusted to achieve approximately 90% infectivity. Selection of infected cells started 48 hours after seeding with puromycin (1 μ g/mL), and clones were either used immediately or harvested, frozen, and stored at -80°C . The cells were left in culture for 24 hours after thawing before starting experiments.

Colony formation

IKK ϵ -depleted PC-3 cells were plated at 1,000 cells per well in 6-well plates and incubated for 24 hours. After 6 days, cells were fixed with methanol and stained with a solution of 50% v/v methanol and 0.5% w/v methylene blue (Sigma-Aldrich). Colonies were counted under a stereomicroscope, and numbers were reported as a percentage of control. Each experiment was repeated three times.

IncuCyte cell proliferation assays

Cells were seeded at a density of 2,000 cells per well in 96-well plates. After 24 hours, cells were treated with BX795 or Amlexanox at different concentrations for 6 days. Cell proliferation was followed by phase contrast microscopy using an IncuCyte Zoom Live-Cell

Imaging System (IncuCyte HD, Essen BioScience). Images were taken every 2 hours for 6 days. Proliferation growth curves were constructed using the cell confluence values established by confluence mask settings determined by the IncuCyte Zoom software.

siRNA transfection

siRNA targeting TBK1 was purchased from Dharmacon. Transient transfection of prostate cancer cells was performed using lipofectamine 2,000 (Invitrogen). Briefly, 400,000 cells were seeded into 6-well plates. After 24 hours, cells were transfected with 5- μ mol/L siRNA for 4 hours. Before transfection, the siRNA was mixed with lipofectamine 2,000 for 20 minutes, according to the manufacturer's instructions. The transfection medium was replaced by RPMI supplemented with 10% FBS. Cells were collected and analyzed 48 hours later.

TLR3 stimulation

Cells were seeded at 500,000 cells in 60-mm plates. After 24 hours, cells were pretreated with 2.5- μ mol/L BX795 for 2 hours before transfection with 10 μ g/mL of the TLR3 agonist pIpC using the lipofectamine 2,000 protocol as described above. After 2 or 4 hours, cells were collected for Western blot experiments.

Western blot analysis

Proteins were obtained from whole cell lysates after a 30-minute incubation at 4°C in lysis buffer (Triton X-100, 50 mmol/L Tris pH 7.4, 150 mmol/L NaCl, 2 mmol/L EDTA, and 10% glycerol) supplemented with a protease inhibitor cocktail (Roche Applied Science) and phosphatase inhibitors (5 mmol/L NaF, 200 μ mol/L Na_3VO_4 , and 100 μ mol/L PMSF). Protein concentrations were quantified by Bradford assay, and 30 μ g of protein per well was separated in 4% to 15% SDS polyacrylamide gels, then transferred onto polyvinylidene difluoride (PVDF) membranes. The antibodies used in this study were anti-IKK ϵ (1/2,000, Imgenex), anti-phospho-IRF-3 (1/3,000, Abcam), anti- β -actin (1/2,000, Abcam), anti-TBK1 (1/1000, Cell Signaling Technology), and anti-IRF-3 (1/800, Santa Cruz).

Cell death and cell-cycle analyses by flow cytometry

Cells were plated at 80,000 cells per well in 6-well plates and incubated for 24 hours. After treatment with 0.75- or 2.5- μ mol/L BX795, the supernatant and adherent cells were collected and pooled. For cell death experiments, cells were washed with PBS and incubated with Annexin V (BD Biosciences) for 25 minutes followed by the addition of DRAQ7 (Abcam) for 5 minutes. Cells were centrifuged, then resuspended in PBS. For cell-cycle experiments, cells were incubated with 100- μ g/mL RNase A and 50- μ g/mL propidium iodide (PI; Sigma Aldrich) for 30 minutes in the dark. Cell staining was analyzed using the Fortessa flow cytometer and the FlowJo 10 software (BD Biosciences).

Senescence-associated- β -galactosidase assay

The senescence-associated (SA)- β -galactosidase assay was performed as previously described (18). Briefly, 20,000 cells were seeded into 24-well plates. After 24 hours, cells were treated with 0.75 or 2.5 μ mol/L BX795 for 6 days. Cells were fixed in formalin (10%), washed with PBS, and incubated overnight at 37°C with fresh staining solution (40 mmol/L citrate acid/sodium phosphate, 150 mmol/L NaCl, 2 mmol/L $\text{Mg}_2\text{Cl}_2 \cdot 6\text{H}_2\text{O}$, 5 mmol/L $\text{K}_4\text{FeCN}_6 \cdot 3\text{H}_2\text{O}$, 5 mmol/L K_3FeCN_6 , and 1 mg/mL X-Gal substrate). The next day, cells were washed with PBS and stained with DAPI. Pictures were taken with bright-field microscopy. Two wells per condition were counted, and

positive blue cells were reported as a percentage of the total cell number.

Total RNA extraction, reverse transcription, and qPCR

Cells were seeded at 100,000 cells per well in 6-well plates, incubated for 24 hours, and treated with 0.75 or 2.5 $\mu\text{mol/L}$ BX795 for 6 days. RNA was extracted with the RNeasy Mini Kit (Qiagen) according to the manufacturer's protocol. RNA concentrations were measured by NanoDrop (Thermo Fisher Scientific) and assessed for purity. For reverse transcription experiments, the Quantitect Reverse Transcription kit (Qiagen) was used with the following conditions: 2 minutes at 42°C, 15 minutes at 42°C, and 3 minutes at 95°C.

qRT-PCR was performed using the SYBR Select Master Mix (Applied Biosystems) in the Applied 63 BioSystems Step One Plus system (UDG activation at 50°C/2 minutes, followed by AmpliTaq activation plus denaturation cycle at 95°C/2 minutes, followed by 40 cycles at 95°C/15 seconds, 60°C/1 minute, and 72°C/30 seconds). Target gene expression was normalized to TATA-box binding protein (TBP) levels. For each sample, the fold change value was expressed as $2^{-\Delta\Delta\text{CT}}$: $\Delta\Delta\text{CT} = (\text{CT}_{\text{target gene}} - \text{CT}_{\text{TBP}})_{\text{control}} - (\text{CT}_{\text{target gene}} - \text{CT}_{\text{TBP}})_{\text{treated}}$. Primers are listed in Supplementary Table S1.

γH2AX foci detection by immunofluorescence

Cells were seeded at 15,000 cells per well onto coverslips in 24-well plates. After 24 hours, cells were treated with 0.75 or 2.5 $\mu\text{mol/L}$ BX795 for 6 days. Then, cells were washed with PBS, fixed with formalin, washed with PBS, permeabilized in PBS containing 0.25% Triton for 20 minutes, and blocked with PBS containing 1% BSA for 30 minutes. Cells were incubated with primary anti- γH2AX antibody (Millipore) for 2 hours. After washing with PBS, cells were incubated with Alexa Fluor Cy5 goat anti-mouse IgG secondary antibody (Life Technologies) for 1 hour. After washing with PBS and water, coverslips were mounted onto slides using ProLong Gold Anti-fade Mountant with DAPI (Life Technologies Inc.). Images (mosaics 4 \times 4) were obtained using a Zeiss AxioObserver Z1 fluorescent microscope (Carl Zeiss). Automated analysis software from Zeiss (AxioVision, Carl Zeiss) was used to count and calculate the average number of foci per nucleus.

5-ethynyl-2'-deoxyuridine detection

Cells were seeded at 15,000 cells per well onto coverslips in 24-well plates and incubated for 24 hours. IKK ϵ -depleted cells or BX795-treated cells were incubated with 10 $\mu\text{mol/L}$ of 5-ethynyl-2'-deoxyuridine (EdU; Invitrogen) overnight at 37°C. After washing with PBS, cells were fixed with formalin for 10 minutes. EdU staining was measured using the reaction solution containing 100 mmol/L Tris pH 8.5, vitamin C, CuSO₄, and Alexa Fluor 647 dye. Cells were incubated with staining solution for 30 minutes in the dark. Next, the cells were washed with PBS, and coverslips were mounted onto slides with ProLong Gold Antifade Mountant with DAPI. Images (mosaics 4 \times 4) were acquired with the Zeiss AxioObserver Z1 microscope and were analyzed with ImageJ software to count the total cell number and positive cells.

Murine xenograft model

All animal experiments complied with all relevant ethical regulations for animal testing and research at Centre de recherche du CHUM (CRCHUM). All experiments were conducted with approval from our institutional committee on animal care [Comité Institutionnel de Protection des Animaux (CIPA)] under protocol number C14011AMMs. Experiments were carried out in 8-week-old male

NODRag1null, IL2rgnull, NOD rag- γ (NRG) mice (from our in-house mouse colony). DU145, PC-3, and 22Rv1 cells were prepared at 1 million cells/200 μL in PBS-matrigel (v/v) and subcutaneously injected into the mouse flank. Mice were weighed once a week, and tumor volumes were measured twice a week. Tumor volumes were calculated using the following equation: $V(\text{mm}^3) = a \times b \times h$, where a is the largest diameter, b is the perpendicular diameter, and h is the height. When xenograft tumor volumes reached between 200 and 300 mm^3 , mice were randomized into three groups: control (carrier: PBS-5% DMSO), BX795 (500 $\mu\text{g/kg}$), or Amlexanox (25 mg/kg). The carrier, BX795, and Amlexanox were administered by intraperitoneal injection every day. Mice were sacrificed when the xenograft tumor volumes reached between 2,000 and 2,500 mm^3 .

Immunofluorescence on xenograft tissue

Tumors were harvested, formalin-fixed, and paraffin-embedded. According to the manufacturer's instructions, 4- μm -thick tissue sections were cut with a microtome and stained using the automated Ventana Discovery XT staining system (Ventana Medical Systems). Antigen retrieval was performed in Cell Conditioning 1 solution, and slides were incubated with anti-Geminin (Proteintech Group) antibodies in PBS at 37°C for 60 minutes. A negative control slide using PBS instead of the primary antibody was prepared in parallel. On the bench, slides were incubated for 20 minutes with blocking solution (Dako, Agilent Technologies) followed by washing with PBS and by incubation with the secondary antibody (anti-rabbit Cy5; Life Technologies Inc.) in PBS at room temperature for 45 minutes. Finally, after washing with PBS, slides were incubated for 15 minutes at room temperature with a 0.1% (w/v) solution of Sudan Black in 70% ethanol to quench tissue autofluorescence. Following a PBS wash, slides were mounted using ProLong Gold Antifade Mountant with DAPI and stored at 4°C. Images were taken with a Zeiss microscope and quantification was performed with ImageJ software.

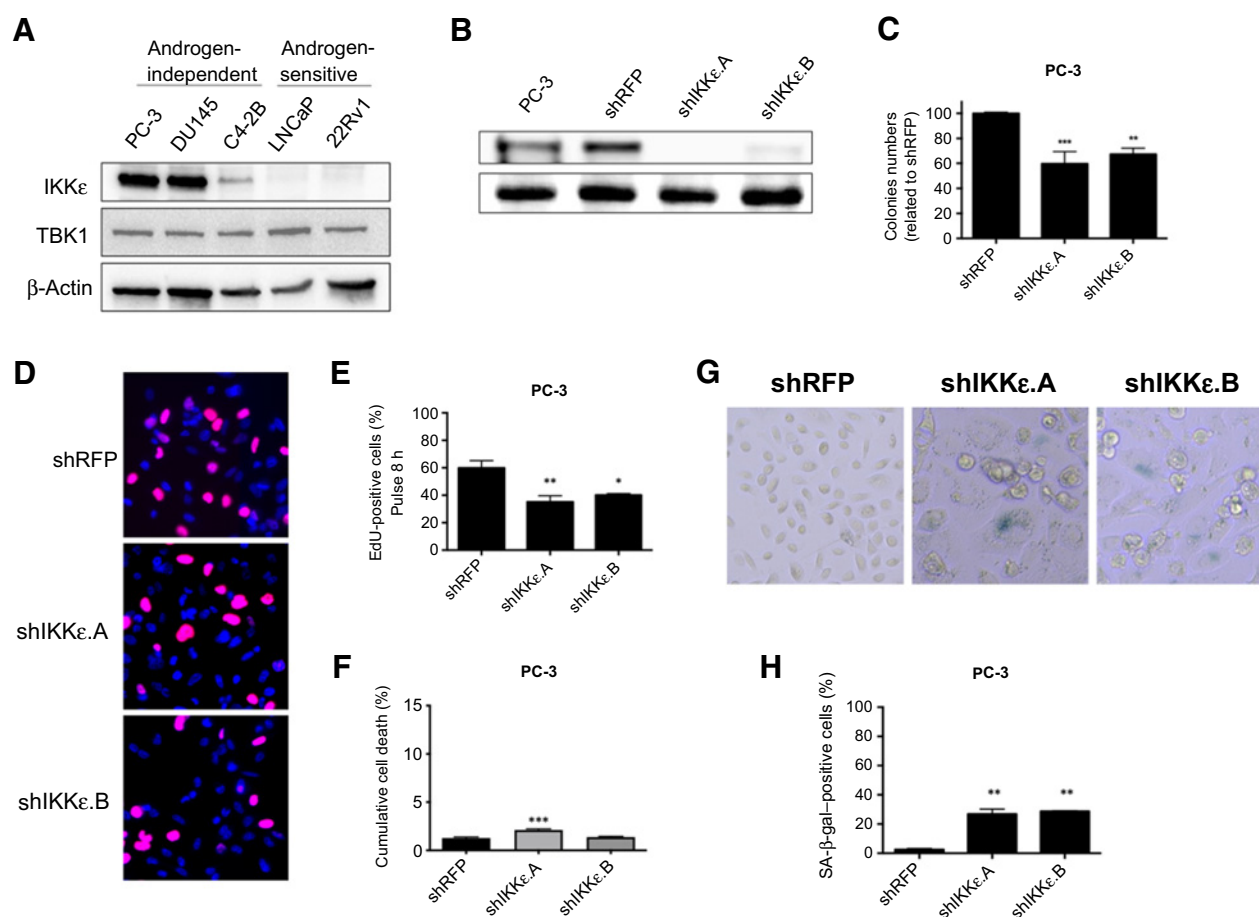
Statistical analysis

Data were expressed as the mean \pm SEM. Statistical analyses were performed using GraphPad Prism 6 software (GraphPad Software). Statistical significance was determined using Student t test or one-way ANOVA and was set at $P = 0.05$. All *in vitro* experiments were repeated at least three times, and the number of mice is indicated for each cohort.

Results

Effect of IKK ϵ knockdown on prostate cancer cell fate decisions

To study the role of IKK ϵ in prostate cancer cell fate decisions, we first verified the reported differences in IKK ϵ expression among our prostate cancer cell lines: androgen-independent prostate cancer cells (PC-3, DU145, and C4-2B) demonstrated IKK ϵ overexpression (Fig. 1A) in comparison with androgen-sensitive prostate cancer cells (LNCaP, 22Rv1) (11). TBK1, the IKK ϵ binding partner in the IFN signaling pathway, was equally expressed in androgen-independent prostate cancer and androgen-sensitive prostate cancer cell lines (Fig. 1A). Although inhibition of IKK ϵ expression decreases PC-3 cell proliferation *in vitro* (12), TBK1 knockdown with siRNA did not affect the proliferation of androgen-independent prostate cancer cell lines (Supplementary Fig. S1). To further understand the IKK ϵ -mediated decrease in cell proliferation, we performed IKK ϵ depletion in PC-3 cells using lentiviral shRNAs (Fig. 1B). Cell-cycle progression was followed using a colony formation assay (Fig. 1C) and short EdU pulse-labeling assays (Fig. 1D and E). Inhibition of IKK ϵ expression

**Figure 1.**

Effect of IKKε knockdown on PC-3 cell fate decision. **A**, IKKε and TBK1 expression levels in prostate cancer cell lines. Whole cell extracts were separated by SDS-PAGE, transferred onto PVDF membranes, and probed with appropriate antibodies. Experiments were performed twice. β-Actin was used as a loading control. **B**, PC-3 cells were transfected with lentiviral shIKKε.A and shIKKε.B. IKKε depletion was confirmed by Western blot analysis. Whole-cell extracts were separated, transferred onto PVDF, and probed with IKKε antibody. **C**, Clonogenic assays were performed on IKKε-depleted PC-3 cells. **D** and **E**, Analysis of 8-hour EdU pulse of PC-3 cells treated at 24 hours posttransfection with either shIKKε.A or shIKKε.B, or with shRFP (control). **D**, Representative images of fixed cells stained with Alexa Fluor 647 dye. Quantification of EdU-positive cells (**E**) performed with ImageJ software. **F**, Cell death analysis of PC3 cells transfected with shIKKε.A and shIKKε.B. Cells were stained with DRAQ7 for 5 minutes and then analyzed by flow cytometry. **G**, Representative images of SA-β-galactosidase activity in IKKε-depleted PC-3 cells or control (shRFP). **H**, Quantification of SA-β-galactosidase activity determined by signal quantification on pictures taken by bright field microscopy. Each experiment was repeated three times. The mean ± SEM of three independent experiments is shown. Data were analyzed using ANOVA. *, $P < 0.05$; **, $P < 0.001$; ***, $P < 0.0001$.

with either shIKKε.A or shIKKε.B significantly decreased colony formation (**Fig. 1C**), and reduced EdU incorporation with a 20% decrease in DNA synthesis (**Fig. 1D** and **E**).

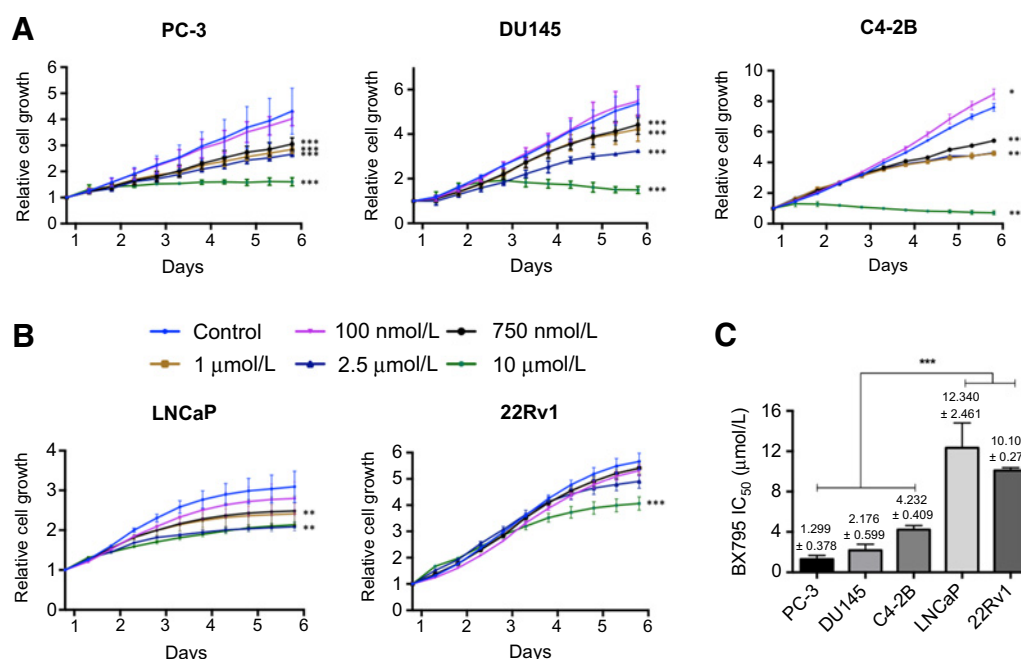
We then evaluated the rate of cell death induced by IKKε depletion in PC-3 cells and observed a slight increase in cell death (<5%) with shIKKε.A, whereas no increase was observed with shIKKε.B (**Fig. 1F**; Supplementary Fig. S2). Inhibition of IKKε also induced a 10.5-fold increase in SA-β-galactosidase activity (**Fig. 1G** and **H**), a specific marker of cellular senescence. These results suggest that lack of IKKε activity induces cell fate decisions that include moderate cell-cycle arrest and a partial senescence phenotype.

Effect of IKKε/TBK1 inhibitor BX795 on prostate cancer cell proliferation

To further characterize prostate cancer cell fate decisions in response to IKKε inhibition, we used a known inhibitor of the

IKKε/TBK1 complex, BX795 (5, 19). First, to detect IKKε activity, cells were treated with the TLR3 agonist pIpC, which leads to the phosphorylation of IRF-3 by the IKKε/TBK1 complex and activates genes in the IFN pathway (Supplementary Fig. S3; ref. 20). After 2 and 4 hours of stimulation with pIpC, IRF-3 phosphorylation was increased in androgen-independent prostate cancer (PC-3, DU145, and C4-2B) and androgen-sensitive prostate cancer (LNCaP and 22Rv1) cell lines. However, phosphorylation was impaired in all cell lines pretreated with 2.5 μmol/L of BX795 (Supplementary Fig. S3), demonstrating that BX795 blocked the IKKε/TBK1 complex activity.

We then examined whether BX795 decreased prostate cancer cell proliferation as efficiently as IKKε depletion in PC-3 cells. Real-time imaging of proliferation assays confirmed a concentration-dependent inhibition of androgen-independent prostate cancer cell proliferation (**Fig. 2A**) when concentrations of BX795 were over 750 nmol/L. At the

**Figure 2.**

Antiproliferative effect of BX795 on androgen-independent prostate cancer cells. Impact of BX795 on androgen-independent prostate cancer (A) and androgen-sensitive prostate cancer (B) cell proliferation. Cells were incubated in 96-well plates and untreated (control) or treated with different concentrations of BX795. Cell growth was followed by IncuCyte live-cell imaging for 6 days. C, Prostate cancer cell sensitivity (IC₅₀) to BX795 was calculated using the AUC of proliferation assays. Bars represent the average of IC₅₀ values (\pm SEM) from three independent experiments. Data were analyzed using ANOVA. *, $P < 0.05$; **, $P < 0.001$; ***, $P < 0.0001$.

highest concentration (10 μ mol/L), proliferation was blocked for all androgen-independent prostate cancer cell lines, and cell numbers even decreased for DU145 and C4-2B (Fig. 2A). At 100 nmol/L, a slight increase in C4-2B cell proliferation was noted. In contrast, the effect of BX795 on androgen-sensitive prostate cancer cell proliferation (LNCaP and 22Rv1) appeared limited (Fig. 2B). Although proliferation of LNCaP decreased (0.8-fold) at concentrations greater than 1 μ mol/L, cells were more resistant to treatment than the androgen-independent prostate cancer cell lines (Fig. 2B and C) and growth was not arrested, even at 10 μ mol/L. Proliferation of 22Rv1 cells was only affected when BX795 concentrations reached 10 μ mol/L (Fig. 2B). Using the AUC, the IC₅₀ of BX795 was calculated for each cell line and revealed that androgen-independent prostate cancer cells had a significantly lower IC₅₀ (1.3 μ mol/L, 2.2 μ mol/L, and 4.2 μ mol/L for PC-3, DU145, and C4-2B, respectively) than androgen-sensitive prostate cancer cells (12.3 μ mol/L and 10.1 μ mol/L for LNCaP and 22Rv1, respectively; Fig. 2C).

In addition, we examined whether BX795 influences the proliferation of a normal prostate cell line, PZ-HPV-7. We monitored IKK ϵ expression by Western blot. As expected, we do not observe constitutive expression of IKK ϵ in PZ-HPV-7 cells (Supplementary Fig. S4). Moreover, real-time imaging assays of proliferation showed that BX795 does not have a significant effect on PZ-HPV-7 proliferation (Supplementary Fig. S4).

These results show that BX795 has a powerful antiproliferative effect on androgen-independent prostate cancer cells compared with androgen-sensitive prostate cancer cells. To characterize this effect, two BX795 concentrations were selected for further study: 0.75 and 2.5 μ mol/L.

BX795 treatment induces a senescence-like phenotype in androgen-independent prostate cancer cells

Because IKK ϵ depletion induced a senescence phenotype in PC-3 cells (Fig. 1), we examined whether BX795 could also induce senescence in androgen-independent prostate cancer cells. Using flow cytometry, cell-cycle progression was analyzed after 6 days of treatment. No effect was observed with 0.75 μ mol/L BX795 in all cell lines except for a low but significant G₂-M phase accumulation in PC-3 cells (Fig. 3A and B; Supplementary Fig. S4A and S4B). However, at 2.5 μ mol/L BX795, the cell-cycle distribution was significantly altered in all cell lines. Moreover, under these conditions, a subpopulation of cells with abnormal DNA content (8N) appeared (Fig. 3A; Supplementary Fig. S5A) in all AnRPC cell lines, with DU145 showing the highest levels. Even with a delayed G₂-M phase, this 8N subpopulation was not observed in androgen-sensitive prostate cancer cell lines (Fig. 3B; Supplementary Fig. S5B).

We then evaluated the apoptosis levels of cells after 6 days of BX795 treatment by flow cytometry. At 0.75 μ mol/L BX795, no increase of cell death was observed for all prostate cancer cell lines (Supplementary Fig. S5). At 2.5 μ mol/L BX795, apoptosis (cumulative AnnexinV/DRAQ7-positive cells) was significantly increased by 2.8-, 5.3-, 7-, 4.3-, and 4.2-fold for PC-3, DU145, C4-2B, LNCaP, and 22Rv1 cells, respectively (Supplementary Fig. S6).

Real-time imaging revealed changes in morphology of androgen-independent prostate cancer cells treated after BX795 treatment. We confirmed cell enlargement using flow cytometry analysis of cell size (forward scatter) and cell granularity (side scatter) in two distinct cell populations: population 1 (normal size) and population 2

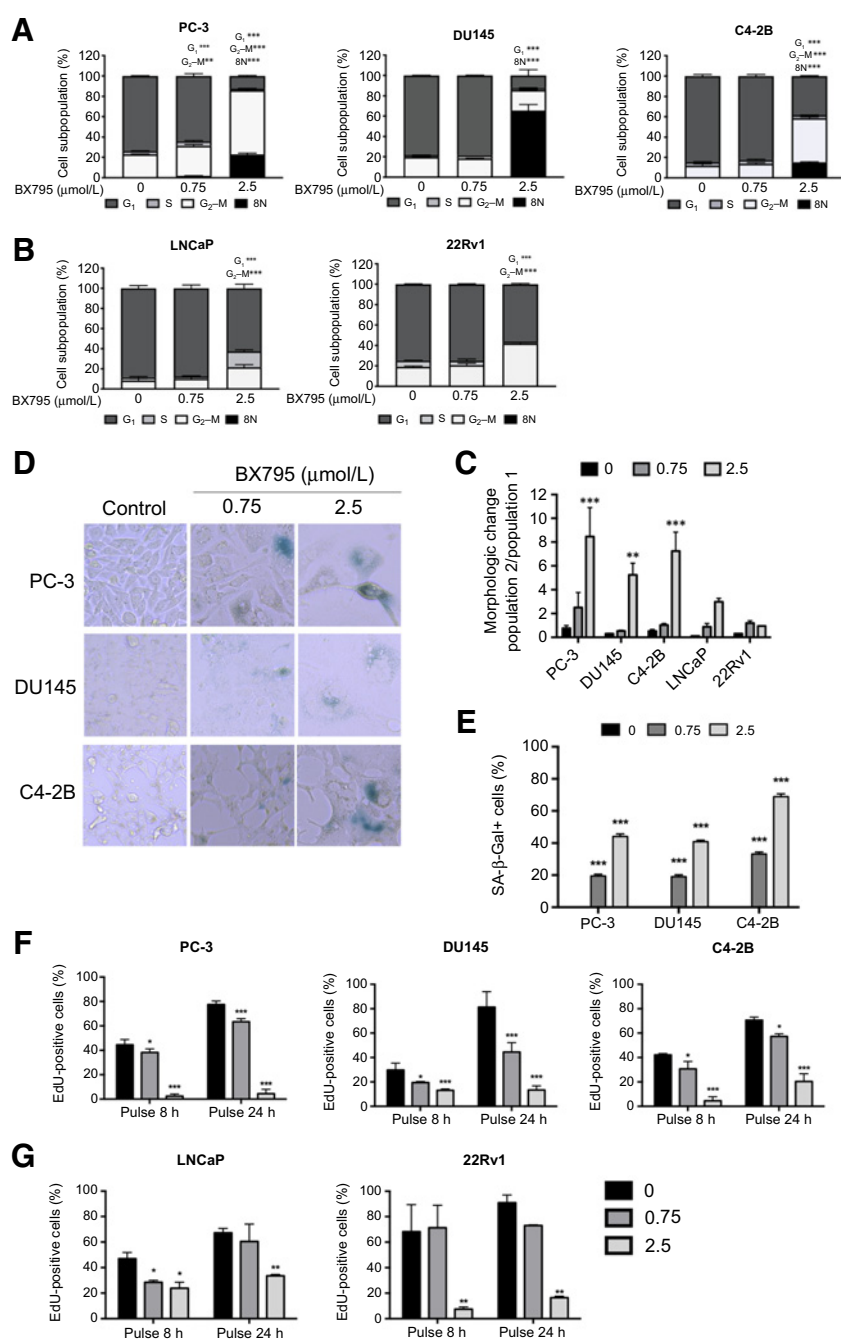


Figure 3.

BX795 induces a senescence-like phenotype in androgen-independent prostate cancer cells. Flow cytometry analyses of cell-cycle populations following 6 days exposure to 0.75 μmol/L or 2.5 μmol/L BX795 of androgen-independent prostate cancer (A) or androgen-sensitive prostate cancer (B) cells. Cells were collected, permeabilized, stained with PI for 30 minutes and analyzed by flow cytometry. C, Prostate cancer cell morphology analyzed by flow cytometry after 6 days of treatment with 0.75 or 2.5 μmol/L BX795. D and E, SA-β-galactosidase activity in androgen-independent prostate cancer and androgen-sensitive prostate cancer cell lines treated with 0.75 μmol/L or 2.5 μmol/L of BX795 for 6 days. Gal, galactosidase. Representative pictures (D) were taken after cell fixation, and SA-β-galactosidase activity was evaluated by signal quantification on pictures taken by bright-field microscopy. For quantification of SA-β-galactosidase-positive cells (E), 100 cells per well (two wells per conditions) were analyzed. F and G, Quantification of EdU-positive cells from 8-hour or 24-hour pulses of EdU in androgen-independent prostate cancer (F) or androgen-sensitive prostate cancer (G) cells after 6 days of BX795 treatment. Cells were fixed and stained with Alexa Fluor 647 dye. Pictures were taken with a Zeiss microscope, and quantification was performed with ImageJ software. Data are the mean ± SEM of three independent experiments analyzed using ANOVA. *P < 0.05; **P < 0.001; ***P < 0.0001.

(enlarged cells; Fig. 3C; Supplementary Fig. S5D and S5E). We observed a significant increase in the ratio of enlarged versus normal-sized cells in 2.5 μmol/L BX795-treated androgen-independent prostate cancer cells at day 6 (Fig. 3C; Supplementary Fig. S5D). Moreover, this trend was also observed in 2.5 μmol/L BX795-treated LNCaP cells (Fig. 3C; Supplementary Fig. S5E). This cell enlargement is consistent with a senescence phenotype.

Following 6 days of treatment with 0.75 μmol/L BX795, β-galactosidase-positive cells were observed in 20% of PC-3 and DU145 cells, and 30% of C4-2B cells (Fig. 3D and E). Treatment with 2.5 μmol/L BX795 resulted in higher levels of positive cells with 40% for PC-3 and DU145 cells and 70% for C4-2B (Fig. 3D and E). In androgen-

sensitive prostate cancer cells (LNCaP and 22Rv1), β-galactosidase-positive cells were not detected after 6 days with either 0.75 or 2.5 μmol/L BX795 (Supplementary Fig. S5C).

To confirm the senescence-like phenotype induced in androgen-independent prostate cancer cells in response to BX795 treatment, EdU pulse-labeling was used to follow SA proliferation arrest, a key hallmark of senescence. Treatment with 0.75 μmol/L BX795 in androgen-independent prostate cancer showed a significant decrease in DNA synthesis (short 8 h EdU pulse) after 6 days, but not a complete proliferation arrest as observed with a longer 24-hour EdU pulse (Fig. 3F; Supplementary Fig. S7). In contrast, 2.5 μmol/L BX795 induced stronger arrests of DNA synthesis in androgen-

independent prostate cancer cells with short or long pulses; only 5% (PC-3), 12% (DU145), and 5% (C4-2B) of cells were positive after a long EdU pulse (Fig. 3F; Supplementary Fig. S7). Compared with androgen-independent prostate cancer cells untreated or treated with 0.75 $\mu\text{mol/L}$, treatment with 2.5 $\mu\text{mol/L}$ BX795 decreased cell-cycle progression at 16-, 6-, and 3.5-fold for PC-3, DU145, and C4-2B, respectively (Fig. 3F; Supplementary Fig. S7). In androgen-sensitive prostate cancer cells, 0.75 $\mu\text{mol/L}$ BX795 did not alter DNA synthesis (short EdU pulse) or the cell cycle (long EdU pulse) in 22Rv1 cells (Fig. 3G; Supplementary Fig. S7). In LNCaP cells, the same treatment only affected DNA synthesis. With 2.5 $\mu\text{mol/L}$ BX795 treatment, DNA synthesis decreased by two- and ninefold for LNCaP and 22Rv1, respectively. Also, this treatment altered cell-cycle progression with a decrease of two- and 5.5-fold for LNCaP and 22Rv1, respectively (Fig. 3G; Supplementary Fig. S7).

These results indicate that treatment with 0.75 $\mu\text{mol/L}$ BX795 was capable of inducing a senescence-like phenotype in androgen-independent prostate cancer cell lines, whereas a higher concentration of 2.5 $\mu\text{mol/L}$ induced abnormal DNA (8N) content and cell death. In androgen-sensitive prostate cancer cells, both BX795 concentrations did not induce a senescence phenotype, but only 2.5 $\mu\text{mol/L}$ BX795 decreased cell-cycle progression and induced cell death.

BX795-induced senescence features are associated with DNA damage and cyclin-dependent kinase inhibitor overexpression

Increased DNA damage is often associated with the induction of senescence (21). To determine whether the senescence phenotype induced by BX795 was associated with DNA damage, we assessed the presence and accumulation of γH2AX foci, a marker of DNA double-strand breaks (22), by immunofluorescence (IF) after 6 days of treatment. At 0.75 $\mu\text{mol/L}$ BX795, the number of γH2AX foci increased fourfold in PC-3 and DU145 cells (Fig. 4A and B), but no increase was observed in C4-2B cells (Fig. 4B; Supplementary Fig. S8A). At 2.5 $\mu\text{mol/L}$ BX795, the number of γH2AX foci increased substantially in all androgen-independent prostate cancer cells (10-, 17-, and sevenfold in PC-3, DU145, and C4-2B cells, respectively). In contrast, neither concentration of BX795 induced any increase of γH2AX foci in androgen-sensitive prostate cancer cells (LNCaP and 22Rv1) after 6 days (Fig. 4B; Supplementary Fig. S8B).

We hypothesized that this increased DNA damage was associated with genomic instability, which is characterized by an accumulation of micronuclei and multinuclei structures (23). At 0.75 $\mu\text{mol/L}$ BX795, 20% of PC-3 and DU145 cells and 10% of C4-2B cells were positive for micronuclei and multinuclei structures, indicating genomic instability (Fig. 4C; Supplementary Fig. S9). At 2.5 $\mu\text{mol/L}$ BX795, an increase in genomic instability was demonstrated by 80%, 95%, and 75% of PC-3, DU145, and C4-2B cells, respectively (Fig. 4C; Supplementary Fig. S9). Micronuclei and multinuclei structures were not detected in androgen-sensitive prostate cancer cells LNCaP and 22Rv1 at either BX795 concentrations (Fig. 4C).

Alterations in cell-cycle progression (Fig. 3A and B) implicate cell-cycle regulators such as cyclin-dependant kinase inhibitors (CDKis). CDKis block cell-cycle progression by inhibiting cyclin and CDK interactions, and their overexpression is also a marker of senescence (24). CDKi expression was followed by qRT-PCR after 6 days of BX795 treatment and showed differences between cell lines (Fig. 4D and E). PC-3 cells treated with 2.5 $\mu\text{mol/L}$ BX795 showed a significant increase in CDKN2B (p15) and CDKN1A (p21) expression levels compared with the untreated control (Fig. 4D). The same BX795 concentration in DU145 cells showed a significant increase in p15 and

p16 expression levels (Fig. 4D). In C4-2B cells, p21, p16, and p15 were significantly overexpressed compared with the control (Fig. 4D). For androgen-sensitive prostate cancer cells (LNCaP and 22Rv1), only p21 expression was increased at 2.5 $\mu\text{mol/L}$ BX795 (Fig. 4E), whereas p16 and p15 expression levels did not change after BX795 treatments (Fig. 4E).

IKK ϵ inhibition delayed tumor growth in a mouse prostate cancer xenograft model

To ensure the activity we observed with BX795 was specific to IKK ϵ , we evaluated the effect of BX795 on IKK ϵ -depleted PC-3 cells by clonogenic and SA- β -galactosidase assays. The results suggest that at a dose of 0.75 $\mu\text{mol/L}$ BX795 inhibition appears to be IKK ϵ -specific. In contrast, at 2.5 $\mu\text{mol/L}$ BX795 (Supplementary Fig. S10), we did not see off-target activity. To ensure specificity *in vivo*, we used an FDA-approved IKK ϵ inhibitor, Amlexanox, to evaluate the impact of IKK ϵ inhibition on tumor growth in a mouse model. First, we validated its activity *in vitro* to ensure that Amlexanox induced the same cell fate decisions observed with BX795 in androgen-independent prostate cancer and androgen-sensitive prostate cancer cells. Androgen-independent prostate cancer cell proliferation significantly decreased at 50, 100, and 200 $\mu\text{mol/L}$ Amlexanox for PC-3, DU145, and C4-2B cells, respectively (Supplementary Fig. S11A), whereas androgen-sensitive prostate cancer proliferation (LNCaP and 22Rv1) was not altered by similar Amlexanox treatment (Supplementary Fig. S11B). In addition, 100 $\mu\text{mol/L}$ Amlexanox significantly increased SA- β -galactosidase activity in PC-3 and DU145 cells (Supplementary Fig. S11C and S11D). At 200 $\mu\text{mol/L}$ Amlexanox, SA- β -galactosidase activity was increased for all androgen-independent prostate cancer cell lines (Supplementary Fig. S11C and S11D). In contrast, androgen-sensitive prostate cancer cells did not demonstrate any SA- β -galactosidase activity at either Amlexanox concentration (Supplementary Fig. S11E). These results confirm that Amlexanox treatment had a comparable effect to BX795 in androgen-independent prostate cancer cells: decreased cell proliferation and increased senescence phenotype.

To investigate the potential effects of BX795 or Amlexanox on prostate cancer tumor growth in a mouse model, subcutaneous androgen-independent prostate cancer xenografts using PC-3 and DU145 cell lines and an androgen-sensitive prostate cancer xenograft using 22Rv1 cells were established. About 2 or 3 weeks after prostate cancer cell injection, mice were treated with a daily dose of 500 $\mu\text{g/kg}$ BX795 or 25 mg/kg Amlexanox for 4 weeks (or with the carrier as a control). There was no observable effect of BX795 or Amlexanox on the weight or behavior of the mice (Supplementary Fig. S12). PC-3 and DU145 tumor growth were significantly reduced by BX795 and Amlexanox treatments compared with the control group (Fig. 5A and B; Supplementary Fig. S13). In comparison, BX795 and Amlexanox did not affect the 22Rv1 tumor growth, which remained comparable with the control group. To validate the antiproliferative effects of BX795 and Amlexanox in our xenograft model, Geminin (GMNN) staining was performed on the harvested xenograft tissue and analyzed by IF, as described by Wohlschlegel and colleagues (25). BX795 treatment altered the cell cycle in androgen-independent Geminin (GMNN) xenografts, indicated by the proliferation-associated GMNN staining that showed a decrease by 1.4- and 1.7-fold in PC-3 and DU145 xenografts, respectively. Similarly, GMNN staining decreased by 1.6- and twofold in Amlexanox-treated PC-3 and DU145 xenografts, respectively (Fig. 5D-G). In 22Rv1 xenografts, GMNN expression was not altered by BX795 as the number of positive cells were similar in both treatment and control groups (Fig. 5H and I), and

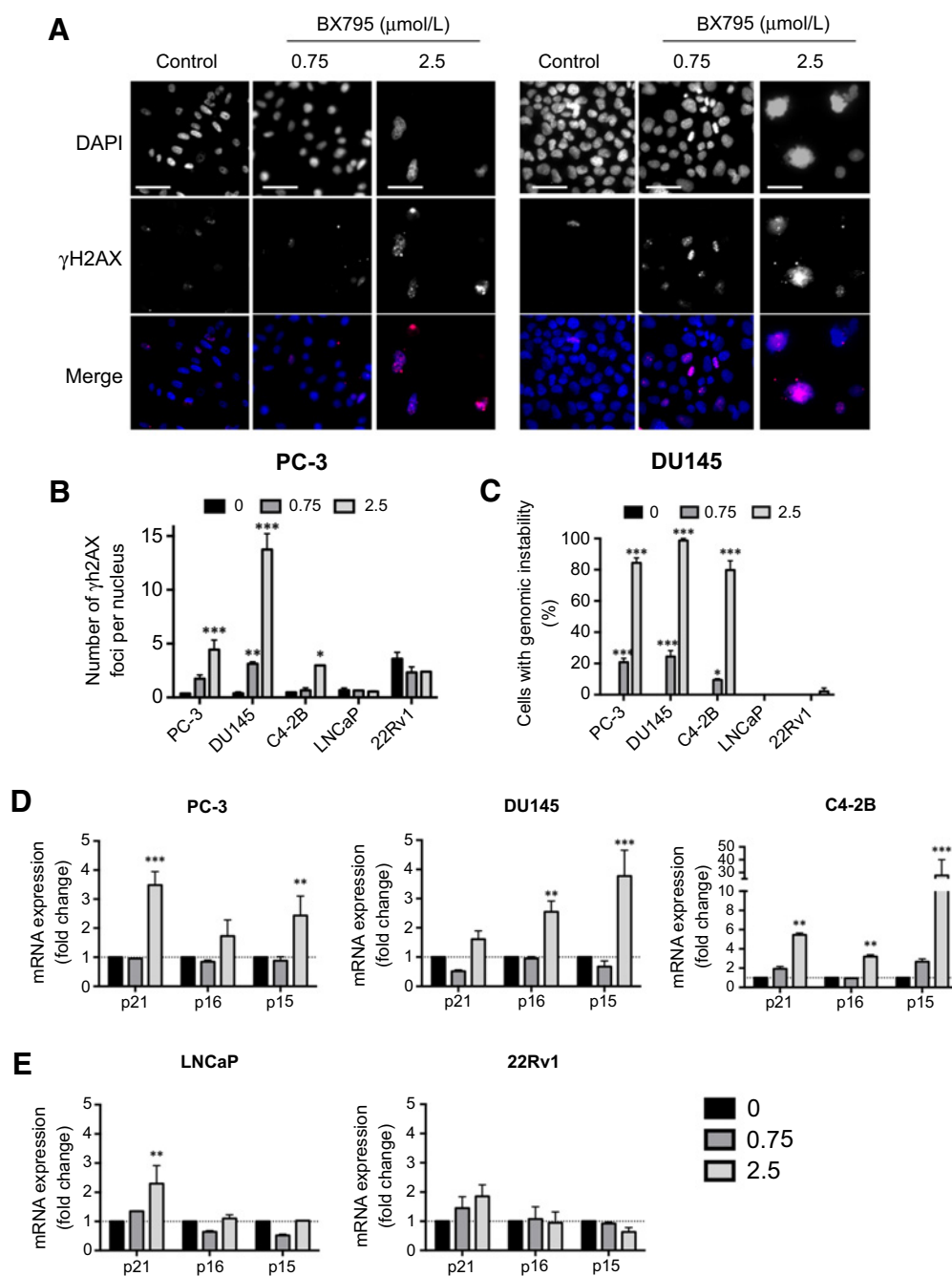


Figure 4.

DNA damage and CDKi overexpression induce senescence phenotype in androgen-independent prostate cancer cells. **A** and **B**, Quantification of DNA damage from BX795 treatment. androgen-independent prostate cancer and androgen-sensitive prostate cancer cells were treated with 0.75 $\mu\text{mol/L}$ or 2.5 $\mu\text{mol/L}$ of BX795 for 6 days. Cells were fixed, γH2AX foci (red) were stained by IF, and nuclei were stained with DAPI (blue). Pictures were taken using a Zeiss microscope (**A**) and are representative of triplicates. The number of γH2AX foci per nucleus (**B**) was counted using AxioVision. **C**, Impact of BX795 treatment on genomic instability. Number of prostate cancer cells containing micronuclei and multinuclei structures after 6 days of 0.75 $\mu\text{mol/L}$ or 2.5 $\mu\text{mol/L}$ BX795 was calculated from pictures acquired from the DAPI channel. CDKi expression in androgen-independent prostate cancer (**D**) and androgen-sensitive prostate cancer cells (**E**) measured by qRT-PCR after 6 days of BX795 treatment. Each experiment was repeated three times. Statistical significance was determined by *t* test for **C** and two-way ANOVA for **D** and **E**. *, $P < 0.05$; **, $P < 0.001$; ***, $P < 0.0001$.

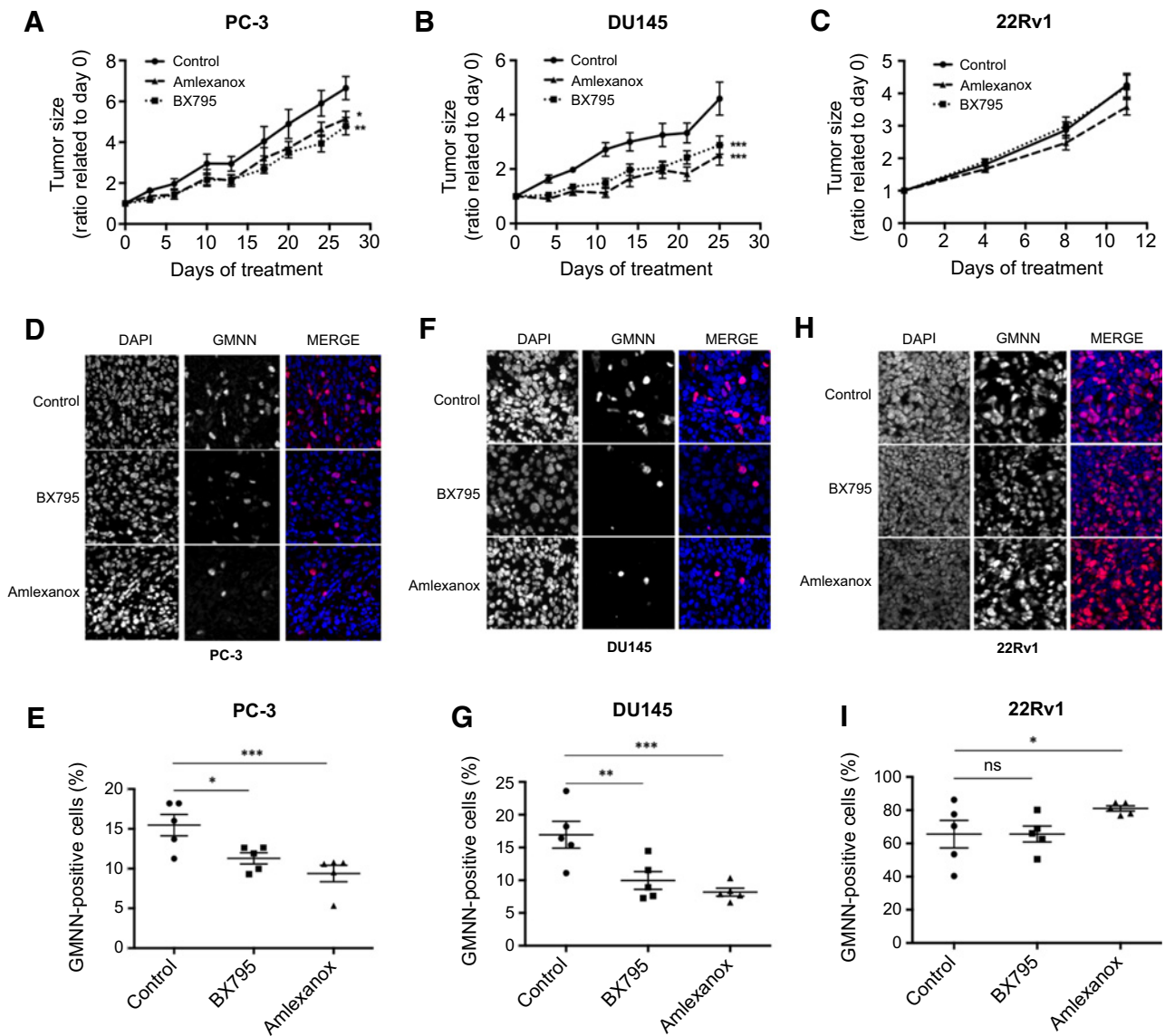


Figure 5. IKK ϵ inhibitors impair tumor growth in xenograft mouse model. Tumor size ratio between the first and last days of treatment for PC-3 (A), DU145 (B), and 22Rv1 (C) xenograft tumors ($n = 9$). BX795 (500 $\mu\text{g}/\text{kg}$) or Amlexanox (25 mg/kg) was administered daily by intraperitoneal delivery. Tumor size was monitored twice a week for the duration of experiments, and all mice were sacrificed at endpoint (tumor size $> 2,000 \text{ mm}^3$). Representative images (D, F, and H) and quantification (E, G, and I) of percentage of GMNN-positive cells in PC-3 (D and E), DU145 (F and G), and 22Rv1 (H and I) xenografts ($n = 5$ per condition). Statistical significance was determined by two-way ANOVA. *, $P < 0.05$; **, $P < 0.001$; ***, $P < 0.0001$.

Amlexanox treatment showed only a slight increase (1.2-fold) in GMNN staining (Fig. 5H and I).

Discussion

Androgen-independent prostate cancer cell lines (PC-3, DU145, and C4-2B) have characteristics close to CRPC tumors in patients. These cell lines show a constitutive activity of NF- κB and overexpress IKK ϵ . Although androgen-sensitive prostate cancer cell lines (LNCaP, 22Rv1) are similar to HSPC tumors as express AR and respond to androgen signaling. We have previously shown that IKK ϵ expression correlates with the aggressiveness of prostate cancer in patients (9) and

that IKK ϵ expression is inducible in androgen-sensitive prostate cancer cell lines, while it is constitutively overexpressed in androgen-independent prostate cancer cells (12). In this study, we show that C4-2B cells, an androgen-independent prostate cancer cell line derived from the IKK ϵ -inducible androgen-sensitive prostate cancer LNCaP cell line (26), display IKK ϵ overexpression. These results support the premise that IKK ϵ expression is a key factor in prostate cancer progression. We also show that IKK ϵ depletion slows proliferation and induces moderate SA- β -galactosidase activity in PC-3 cells. Inhibition of the IKK ϵ /TBK1 complex by BX795 or Amlexanox decreased proliferation in androgen-independent prostate cancer cell lines and induced features of senescence accompanied by induction of

DNA damage and genomic instability in androgen-independent prostate cancer cells. Unlike true senescence, this effect appears to be reversible, a characteristic that has previously been identified in cancer cells (17). In contrast, these inhibitors had a limited antiproliferative effect on androgen-sensitive prostate cancer cell lines, and BX795 did not induce a senescence phenotype in these cells. Finally, treatment with BX795 and Amlexanox delayed androgen-independent prostate cancer tumor growth in mouse models but had no effect on 22Rv1 (androgen-sensitive prostate cancer) xenograft growth. The IKK ϵ inhibitors seem only efficient against androgen-independent prostate cancer cell lines. Although there are many drugs that target HSPC tumors, in the CRPC setting, there are few therapeutic strategies and none that are curative, highlighting the importance of targeting this stage of the disease.

A variety of cancers, including lung, breast, melanoma, pancreatic, bladder, and colon cancers, demonstrate overexpression of TBK1, which is the binding partner of IKK ϵ (27–30). TBK1 plays an important role in oncogenic transformation in melanoma, breast, and lung cancers (31–33) and may also play a role in drug resistance. For example, TBK1 overexpression in breast cancer is correlated with tamoxifen resistance (33) and is associated with resistance to BRAF (31) or MEK inhibitors (28) in melanoma. TBK1 inhibition by BX795 increases the sensitivity of breast cancer cells to tamoxifen treatment (33) and has an antiproliferative effect in human oral squamous cell carcinoma (34). BX795 also inhibits TBK1 enhancement of bladder cancer cell proliferation and migration (35). Moreover, IKK ϵ /TBK1 inhibition by Amlexanox inhibits melanoma proliferation (36) and potentiates the antitumor and antimetastatic effects of docetaxel in breast cancer (37). Although BX795 and Amlexanox reduced androgen-independent prostate cancer tumor size and *in vitro* cell growth, we showed that this was not specifically associated with TBK1 because TBK1 knock-down had no impact on androgen-independent prostate cancer cell proliferation (Supplementary Fig. S1). In contrast, IKK ϵ depletion significantly decreased androgen-independent prostate cancer proliferation [(12) and Fig. 1]. Based on these results, we suggest that the effect of BX795 and Amlexanox in androgen-independent prostate cancer cell lines were not due to TBK1 inhibition but is principally related to IKK ϵ inhibition.

BX795 was originally developed as a PDK1 inhibitor but functions more effectively as an inhibitor of the IKK ϵ /TBK1 complex (19). Although previous studies have reported that BX795 had multiple off-target effects, such as the Aurora, AKT (34), TAK1, JNK, or MKK4 (38), our results showed that BX795 can show high specificity to inhibit IKK ϵ activity at appropriate doses. We observe that BX795 induces a phenotype of senescence accompanied by genomic instability only in androgen-independent prostate cancer cells (PC-3, DU145, and C4-2B cells) for which IKK ϵ expression is constitutive. In the LNCaP and 22Rv1 lines, where IKK ϵ expression is only inducible, we do not observe cell senescence, genomic instability, or DNA damage. Furthermore, we showed in our study that BX795 treatment replicated the effect of IKK ϵ depletion by shRNA on PC-3 cells (i.e., increase of SA- β -galactosidase activity and cell growth arrest). In fact, BX795 treatment at low (0.75 μ mol/L) and high (2.5 μ mol/L) concentrations produced two different phenotypes in androgen-independent prostate cancer cells. At 0.75 μ mol/L, BX795 induced a moderate senescence in androgen-independent prostate cancer cells, accompanied by slower cell growth with an increase of γ H2AX foci and about 20% of cells showing micronuclei and multi-nuclei structures. At 2.5 μ mol/L of BX795, growth arrest and a senescence phenotype were observed in a greater proportion

of androgen-independent prostate cancer cells of which about 80% of cells showed genomic instability and a significant accumulation of DNA damage with an increase of cell death. Because IKK ϵ depletion and 0.75 μ mol/L BX795 treatment induce a comparable, moderate senescence in PC-3 cells, and a higher BX795 concentration induces a stronger senescence phenotype with genomic instability, we suggest that increasing BX795 intensifies the effect of inducing a senescence phenotype in an IKK ϵ -dependent manner. In support of this notion, our specificity experiments show that 0.75 μ mol/L BX795 is a specific dose inhibiting IKK ϵ activity. Likewise, Amlexanox, an IKK ϵ inhibitor with better specificity for IKK ϵ than BX795, also induces a senescence phenotype similar to BX795. Amlexanox is an FDA-approved drug for the treatment of aphthous ulcers and shows the same *in vivo* antitumor effect as BX795. Notably, IKK ϵ inhibitors have no effect on the proliferation or induction of senescence in androgen-sensitive prostate cancer cells, which do not constitutively express IKK ϵ . Therefore, these observations support the hypothesis that BX795 and Amlexanox induce a senescence phenotype via IKK ϵ in androgen-independent prostate cancer cell lines.

Previously, we have shown that IKK ϵ overexpression activates IL6 and IL8 secretion, whereas IKK ϵ depletion inhibits their expression (12, 39). High concentrations of these cytokines may also exist in the SASP of senescent cells, including androgen-independent prostate cancer cells (40). This excess in IL6 and IL8 may enhance the growth of neighboring nonsenescent androgen-independent prostate cancer cells through activation of the androgen receptor in a STAT3-dependent manner leading to cell proliferation (41, 42). Moreover, the upregulation of IL6 and activation of STAT3 lead to crucial mechanisms of therapeutic resistance in cancer cells (43, 44). These observations suggest that IKK ϵ may contribute to androgen-independent prostate cancer progression through IL6 and IL8 upregulation.

C/EBP- β is a key senescence regulator that represses and activates different senescence genes in a context-dependent manner (45) and induces the expression of SASP genes, including IL6 and IL8 (45). Numerous studies have shown that C/EBP- β is involved in diverse functions such as inflammation, cellular differentiation, cell survival, tumor invasiveness, and growth arrest (46–51). In prostate cancer, C/EBP- β is activated by IKK ϵ and induces IL6 and IL8 secretion that is associated with inflammatory prostate cancer progression (12). C/EBP- β expression was shown to be high in patients with HSPC, and upon androgen deprivation, C/EBP- β levels rapidly increased in androgen-sensitive prostate cancer cell lines (9, 52). In addition, androgen deprivation induces a senescence phenotype (ADIS) associated with tumor-promoting traits that lead to prosurvival mechanisms (10, 16, 52, 53). Our observations and data from the literature suggest a mechanism of ADT resistance influenced by IKK ϵ . The induction of ADIS leads to IL6 and IL8 secretion via C/EBP- β activation (40, 52). When ADT resistance sets in, IL6 and IL8 levels continue to be high, thereby contributing to prosurvival mechanisms, cell proliferation and ultimately castrate resistance. Because proliferating androgen-independent prostate cancer cells no longer benefit from the SASP, they would normally reduce IL6 and IL8 secretion. However, we propose that androgen-independent prostate cancer cells start to constitutively express IKK ϵ to activate C/EBP- β , thus driving IL6/IL8 secretion independent of senescence. Conversely, IKK ϵ inhibition by shRNA or inhibitors, decreases IL6 and IL8 secretions and pushes androgen-independent prostate cancer cells to return to a senescence phenotype.

In addition to its key function in proinflammatory cytokine secretion, C/EBP- β has a role in DNA damage resolution because it

regulates the transcription of genes involved in DNA repair, such as *BRCA1/2*, *ATM*, or *Rad51* (54–56). Importantly, IKKε also plays a role in protecting cells from DNA-damage-induced cell death (57). After genotoxic stress, IKKε translocates to the nucleus, leading to the formation of promyelocytic leukemia nuclear bodies (57). We have shown that IKKε translocates into the nucleus of androgen-independent prostate cancer cells (39). This prosurvival function of IKKε in the nucleus is dependent on the phosphorylation of IKKε itself and its targets, which include *C/EBP-β* (57). Our results showing DNA damage accumulation in response to BX795 treatment support the following hypothesis: nuclear IKKε activity increases *C/EBP-β* activation, which promotes DNA repair mechanisms that may allow the cancer cell to either be protected from ADIS and/or promote resistance to ADIS.

We have previously shown that IKKε depletion decreased cell proliferation *in vitro* and *in vivo* in PC-3 cells (12). In this study, we demonstrated that IKKε inhibitors induced a senescence phenotype and genomic instability in androgen-independent prostate cancer cell lines. We validated that IKKε inhibitors delayed androgen-independent prostate cancer tumor growth in mouse models. These observations add to previous evidence suggesting that IKKε allows prostate cancer cells to progress to an androgen-independent or castrate-resistant state by escaping ADIS, possibly through the activation of *C/EBP-β*, which induces DNA damage repair and *IL6/IL8* secretion. Together, this supports the therapeutic potential of IKKε for the treatment of patients with CRPC, as well as for the prevention of early-onset prostate cancer progression in combination with ADT.

Authors' Disclosures

No disclosures were reported.

References

1. Lonergan PE, Tindall DJ. Androgen receptor signaling in prostate cancer development and progression. *J Carcinog* 2011;10:20.
2. Saraon P, Jarvi K, Diamandis EP. Molecular alterations during progression of prostate cancer to androgen independence. *Clin Chem* 2011;57:1366–75.
3. Culig Z, Santer FR. Androgen receptor signaling in prostate cancer. *Cancer Metastasis Rev* 2014;33:413–27.
4. Sharp A, Coleman I, Yuan W, Sprenger C, Dolling D, Rodrigues DN, et al. Androgen receptor splice variant-7 expression emerges with castration resistance in prostate cancer. *J Clin Invest* 2019;129:192–208.
5. Sharma S, tenOever BR, Grandvaux N, Zhou G-P, Lin R, Hiscott J. Triggering the interferon antiviral response through an IKK-related pathway. *Science* 2003;300:1148–51.
6. Huttu JE, Shen RR, Abbott DW, Zhou AY, Sprott KM, Asara JM, et al. Phosphorylation of the tumor suppressor CYLD by the breast cancer oncogene IKKε promotes cell transformation. *Mol Cell* 2009;34:461–72.
7. Guo J-P, Tian W, Shu S, Xin Y, Shou C, Cheng JQ. IKKε phosphorylation and inhibition of FOXO3a: a mechanism of IKKε oncogenic function. *PLoS One* 2013;8:e63636.
8. Hsu S, Kim M, Hernandez L, Grajales V, Noonan A, Anver M, et al. IKK-ε coordinates invasion and metastasis of ovarian cancer. *Cancer Res* 2012;72:5494–504.
9. Péant B, Forest V, Trudeau V, Latour M, Mes-Masson A-M, Saad F. IkappaB-Kinase-ε (IKKε) expression and localization in prostate cancer tissues. *Prostate* 2011;71:1131–8.
10. Burton DGA, Giribaldi MG, Munoz A, Halvorsen K, Patel A, Jorda M, et al. Androgen deprivation-induced senescence promotes outgrowth of androgen-refractory prostate cancer cells. *PLoS One* 2013;8:e68003.
11. Péant B, Diallo J-S, Lessard L, Delvoe N, Le Page C, Saad F, et al. Regulation of IkappaB kinase ε expression by the androgen receptor and the nuclear factor-kappaB transcription factor in prostate cancer. *Mol Cancer Res* 2007;5:87–94.
12. Péant B, Gilbert S, Le Page C, Poisson A, L'Ecuyer E, Boudhraa Z, et al. IkappaB-Kinase-ε (IKKε) over-expression promotes the growth of prostate cancer through the *C/EBP-β* dependent activation of *IL-6* gene expression. *Oncotarget* 2017;8:14487–501.
13. Collado M, Blasco MA, Serrano M. Cellular senescence in cancer and aging. *Cell* 2007;130:223–33.
14. Hanahan D, Weinberg RA. Hallmarks of cancer: the next generation. *Cell* 2011;144:646–74.
15. Coppé J-P, Desprez P-Y, Krtolica A, Campisi J. The senescence-associated secretory phenotype: the dark side of tumor suppression. *Annu Rev Pathol* 2010;5:99–118.
16. Pernicová Z, Slabáková E, Kharaishvili G, Bouchal J, Král M, Kunická Z, et al. Androgen depletion induces senescence in prostate cancer cells through down-regulation of Skp2. *Neoplasia* 2011;13:526–36.
17. Fleury H, Malaquin N, Tu V, Gilbert S, Martinez A, Olivier M-A, et al. Exploiting interconnected synthetic lethal interactions between PARP inhibition and cancer cell reversible senescence. *Nat Commun* 2019;10:2556.
18. Dimri GP, Lee X, Basile G, Acosta M, Scott G, Roskelley C, et al. A biomarker that identifies senescent human cells in culture and in aging skin *in vivo*. *Proc Natl Acad Sci U S A* 1995;92:9363–7.
19. Clark K, Plater L, Pegg M, Cohen P. Use of the pharmacological inhibitor BX795 to study the regulation and physiological roles of TBK1 and IkappaB kinase ε: a distinct upstream kinase mediates Ser-172 phosphorylation and activation. *J Biol Chem* 2009;284:14136–46.
20. Fitzgerald KA, McWhirter SM, Faia KL, Rowe DC, Latz E, Golenbock DT, et al. IKKε and TBK1 are essential components of the IRF3 signaling pathway. *Nat Immunol* 2003;4:491–6.
21. Rodier F, Muñoz DP, Teachener R, Chu V, Le O, Bhaumik D, et al. DNA-SCARS: distinct nuclear structures that sustain damage-induced senescence growth arrest and inflammatory cytokine secretion. *J Cell Sci* 2011;124:68–81.

Authors' Contributions

S. Gilbert: Conceptualization, validation, investigation, visualization, methodology, writing—original draft. **B. Péant:** Conceptualization, supervision, investigation, writing—original draft. **N. Malaquin:** Visualization, methodology. **V. Tu:** Methodology. **H. Fleury:** Visualization, methodology. **K. Leclerc-Desaulniers:** Methodology. **F. Rodier:** Visualization, methodology. **A.-M. Mes-Masson:** Supervision, funding acquisition, project administration, writing—review and editing. **F. Saad:** Supervision, funding acquisition, project administration, writing—review and editing.

Acknowledgments

We thank the animal facility of the Centre de recherche du CHUM (CRCHUM) for performing all animal experiments as well as the molecular pathology core facility and the Institut du cancer de Montréal (ICM) imaging/live imaging platform for performing IHC staining and scans, respectively. The authors also thank Christine Caron for assisting with the quantification of immunofluorescence signals. F. Rodier, A.-M. Mes-Masson, and F. Saad are researchers of the CRCHUM/ICM, which receives support from the Fonds de recherche en santé (FRQS). F. Rodier was supported by FRQS junior II – senior career awards (33070, 281706). N. Malaquin was supported by a Cancer Research Society (CRS) operating grant to F. Rodier (23464). V. Tu was supported by a FRQS PhD fellowship and received ICM-Canderel excellence awards. S. Gilbert is supported by a studentship from the Canderel Fund of the ICM. F. Saad holds the Université de Montréal Raymond Garneau Chair for Prostate Cancer Research. This work was supported by the Raymond Garneau Chair in Prostate Cancer research and grants from the Canadian Urologic Oncology Group, Prostate Cancer Canada, ICM, and the Cancer Research Society.

The costs of publication of this article were defrayed in part by the payment of page charges. This article must therefore be hereby marked *advertisement* in accordance with 18 U.S.C. Section 1734 solely to indicate this fact.

Received June 10, 2021; revised October 12, 2021; accepted December 17, 2021; published first December 29, 2021.

22. Kuo LJ, Yang LX. Gamma-H2AX - a novel biomarker for DNA double-strand breaks. *In Vivo* 2008;22:305–9.
23. Kalsbeek D, Golsteyn RM. G2/M-phase checkpoint adaptation and micronuclei formation as mechanisms that contribute to genomic instability in human cells. *Int J Mol Sci* 2017;18:2344.
24. Rodier F, Campisi J. Four faces of cellular senescence. *J Cell Biol* 2011;192:547–56.
25. Wohlschlegel JA, Kutok JL, Weng AP, Dutta A. Expression of geminin as a marker of cell proliferation in normal tissues and malignancies. *Am J Pathol* 2002;161:267–73.
26. Thalmann GN, Anezinis PE, Chang SM, Zhou HE, Kim EE, Hopwood VL, et al. Androgen-independent cancer progression and bone metastasis in the LNCaP model of human prostate cancer. *Cancer Res* 1994;54:2577–81.
27. Deng T, Liu JC, Chung PED, Uehling D, Aman A, Joseph B, et al. shRNA kinome screen identifies TBK1 as a therapeutic target for HER2+ breast cancer. *Cancer Res* 2014;74:2119–30.
28. Vu HL, Aplin AE. Targeting TBK1 inhibits migration and resistance to MEK inhibitors in mutant NRAS melanoma. *Mol Cancer Res* 2014;12:1509–19.
29. Ou Y-H, Torres M, Ram R, Formstecher E, Roland C, Cheng T, et al. TBK1 directly engages Akt/PKB survival signaling to support oncogenic transformation. *Mol Cell* 2011;41:458–70.
30. Chien Y, Kim S, Bumeister R, Loo Y-M, Kwon SW, Johnson CL, et al. RalB GTPase-mediated activation of the IkappaB family kinase TBK1 couples innate immune signaling to tumor cell survival. *Cell* 2006;127:157–70.
31. Eskiocak B, McMillan EA, Mendiratta S, Kollipara RK, Zhang H, Humphries CG, et al. Biomarker accessible and chemically addressable mechanistic subtypes of BRAF melanoma. *Cancer Discov* 2017;7:832–51.
32. Cooper JM, Ou Y-H, McMillan EA, Vaden RM, Zaman A, Bodemann BO, et al. TBK1 provides context-selective support of the activated AKT/mTOR pathway in lung cancer. *Cancer Res* 2017;77:5077–94.
33. Wei C, Cao Y, Yang X, Zheng Z, Guan K, Wang Q, et al. Elevated expression of TANK-binding kinase 1 enhances tamoxifen resistance in breast cancer. *Proc Natl Acad Sci U S A* 2014;111:E601–10.
34. Bai L-Y, Chiu C-F, Kapuriya NP, Shieh T-M, Tsai Y-C, Wu C-Y, et al. BX795, a TBK1 inhibitor, exhibits antitumor activity in human oral squamous cell carcinoma through apoptosis induction and mitotic phase arrest. *Eur J Pharmacol* 2015;769:287–96.
35. Chen W, Luo K, Ke Z, Kuai B, He S, Jiang W, et al. TBK1 promote bladder cancer cell proliferation and migration via Akt signaling. *J Cancer* 2017;8:1892–9.
36. Möller M, Wasel J, Schmetzer J, Weiß U, Meissner M, Schiffmann S, et al. The specific IKKepsilon/TBK1 inhibitor amlexanox suppresses human melanoma by the inhibition of autophagy, NF-kappaB and MAP kinase pathways. *Int J Mol Sci* 2020;21:4721.
37. Bishop RT, Marino S, de Ridder D, Allen RJ, Lefley DV, Sims AH, et al. Pharmacological inhibition of the IKKepsilon/TBK-1 axis potentiates the anti-tumour and anti-metastatic effects of Docetaxel in mouse models of breast cancer. *Cancer Lett* 2019;450:76–87.
38. Yu T, Wang Z, Jie W, Fu X, Li B, Xu H, et al. The kinase inhibitor BX795 suppresses the inflammatory response via multiple kinases. *Biochem Pharmacol* 2020;174:113797.
39. Péant B, Diallo J-S, Dufour F, Le Page C, Delvoe N, Saad F, et al. Over-expression of IkappaB-kinase-epsilon (IKKepsilon/IKKi) induces secretion of inflammatory cytokines in prostate cancer cell lines. *Prostate* 2009;69:706–18.
40. Malaquin N, Vancayseele A, Gilbert S, Antenor-Habazac L, Olivier M-A, Ait Ali Brahem Z, et al. DNA damage- but not enzalutamide-induced senescence in prostate cancer promotes senolytic Bcl-xL inhibitor sensitivity. *Cells* 2020;9:1593.
41. Culig Z, Bartsch G, Hobisch A. Interleukin-6 regulates androgen receptor activity and prostate cancer cell growth. *Mol Cell Endocrinol* 2002;197:231–8.
42. Chen T, Wang LH, Farrar WL. Interleukin 6 activates androgen receptor-mediated gene expression through a signal transducer and activator of transcription 3-dependent pathway in LNCaP prostate cancer cells. *Cancer Res* 2000;60:2132–5.
43. Yu H, Lee H, Herrmann A, Buettner R, Jove R. Revisiting STAT3 signalling in cancer: new and unexpected biological functions. *Nat Rev Cancer* 2014;14:736–46.
44. Yang Z, Guo L, Liu D, Sun L, Chen H, Deng Q, et al. Acquisition of resistance to trastuzumab in gastric cancer cells is associated with activation of IL-6/STAT3/Jagged-1/Notch positive feedback loop. *Oncotarget* 2015;6:5072–87.
45. Salotti J, Johnson PF. Regulation of senescence and the SASP by the transcription factor C/EBPbeta. *Exp Gerontol* 2019;128:110752.
46. Sebastian T, Malik R, Thomas S, Sage J, Johnson PF. C/EBPbeta cooperates with RB/E2F to implement Ras(V12)-induced cellular senescence. *EMBO J* 2005;24:3301–12.
47. Poli V. The role of C/EBP isoforms in the control of inflammatory and native immunity functions. *J Biol Chem* 1998;273:29279–82.
48. Choy L, Derynck R. Transforming growth factor-beta inhibits adipocyte differentiation by Smad3 interacting with CCAAT/enhancer-binding protein (C/EBP) and repressing C/EBP transactivation function. *J Biol Chem* 2003;278:9609–19.
49. Heckman CA, Wheeler MA, Boxer LM. Regulation of Bcl-2 expression by C/EBP in t(14;18) lymphoma cells. *Oncogene* 2003;22:7891–9.
50. Oya M, Horiguchi A, Mizuno R, Marumo K, Murai M. Increased activation of CCAAT/enhancer binding protein-beta correlates with the invasiveness of renal cell carcinoma. *Clin Cancer Res* 2003;9:1021–7.
51. Pal R, Janz M, Galson DL, Gries M, Li S, Jöhrens K, et al. C/EBPbeta regulates transcription factors critical for proliferation and survival of multiple myeloma cells. *Blood* 2009;114:3890–8.
52. Barakat DJ, Zhang J, Barberi T, Denmeade SR, Friedman AD, Paz-Priel I. CCAAT/Enhancer binding protein beta controls androgen-deprivation-induced senescence in prostate cancer cells. *Oncogene* 2015;34:5912–22.
53. Ewald JA, Desotelle JA, Church DR, Yang B, Huang W, Laurila TA, et al. Androgen deprivation induces senescence characteristics in prostate cancer cells in vitro and in vivo. *Prostate* 2013;73:337–45.
54. Burke LJ, Sevcik J, Gambino G, Tudini E, Mucaki EJ, Shirley BC, et al. BRCA1 and BRCA2 5' noncoding region variants identified in breast cancer patients alter promoter activity and protein binding. *Hum Mutat* 2018;39:2025–39.
55. Messenger ZJ, Hall JR, Jima DD, House JS, Tam HW, Tokarz DA, et al. C/EBPbeta deletion in oncogenic Ras skin tumors is a synthetic lethal event. *Cell Death Dis* 2018;9:1054.
56. Liu D, Zhang X-X, Li M-C, Cao C-H, Wan D-Y, Xi B-X, et al. C/EBPbeta enhances platinum resistance of ovarian cancer cells by reprogramming H3K79 methylation. *Nat Commun* 2018;9:1739.
57. Renner F, Moreno R, Schmitz ML. SUMOylation-dependent localization of IKKepsilon in PML nuclear bodies is essential for protection against DNA-damage-triggered cell death. *Mol Cell* 2010;37:503–15.